JOURNAL OF APPLIED POLYMER SCIENCE VOL. 12, PP. 2273–2298 (1968)

A Study of Spinnability in the Wet-Spinning of Acrylic Fibers

D. R. PAUL,* *Chemstrand Research Center, Inc., Durham, North Carolina 27702*

Synopsis

An extensive study of spinnability is presented for the formation of acrylic fibers by wet-spinning. The system consisted of an acrylonitrile–vinyl acetate copolymer with dimethylacetamide as the solvent and water in most instances as the nonsolvent. The term spinnability is used here to denote the type of filament breakage that occurs in the spin bath near the spinnerette face as the withdrawal speed V_1 is increased to some critical value. This maximum speed $V_{1,m}$ depends on essentially every spinning variable. Data are presented for a wide range of spinnerette hole diameters, flow rates per hole, coagulation rates, temperatures, and polymer concentration in the spinning solution. The freely extruded velocity of the filaments, V_f, is also given over the same range of variables. The free velocity is much less than the average velocity because of the Barus effect. Some similarities are noted in the response of $V_{1,m}$ and V_f to certain variables. In fact, $V_{1,m}$ seems to be determined by V_f. Through this observation the influence of the Barus effect on spinnability is easily seen. Spinnability is discussed also in terms of coagulation rates. It is concluded that both rheological and coagulation phenomena are important in the breakage mechanism. These observations are probably applicable in part to other wet-spinning systems.

INTRODUCTION

The formation of fibers by wet-spinning proceeds by a very complex mechanism, which involves a combination of rheological and diffusional phenomena that are not altogether understood individually. Recently attempts have been made to study these processes under ideal model situations to learn more about fiber formation. An earlier paper by the author[1] discussed the diffusion that occurs within the filament during coagulation and the resultant conversion of the polymer solution into a fiber. Fitzgerald and Craig[2] have discussed the extrusion of the spinning solution through the spinnerette holes and mentioned briefly the behavior of the filament in the bath. This work is an extension and elaboration of some of these earlier studies. It is concerned primarily with spinnability, or spinning stability, and how it is influenced by the rheological and diffusional phenomena reported earlier. The reader is referred to previous publications[3,4] for familiarization with the wet-spinning process and the resultant fiber to be investigated here.

* Present address: Department of Chemical Engineering, The University of Texas, Austin, Texas 78712.

Spinnability is a frequently used word that is seldom clearly defined. In general, it refers to the ability or the ease of making fibers from a given set of raw materials; however, in practice the word is used to describe everything from drawing out ligaments of a polymer solution from a beaker with a stirring rod to the production of yarns from staple filament. The work is limited here to a very special meaning for a particular process. A description of this spinning stability phenomenon follows.

As in a typical wet-spinning operation, a polymer solution is pumped by a positive displacement pump to a spinnerette with N holes. The weight fraction of polymer in the solution is w_2, and the solution density is ρ. The rate of pumping is adjusted so that the flow rate per hole is Q (in cubic centimeters per minute). The spinnerette is fully immersed in a bath that coagulates the filaments after they emerge from the spinnerette holes. These filaments are removed from the bath by a rotating roll, or godet. Since other godets are involved downstream in the process, this one is called the first godet and its peripheral velocity is called V_1. Now, for a given set of spinning conditions and constant Q we shall see the consequences of varying V_1. First V_1 is set at a low value and then increased slowly. If the increases are made slowly enough, the system will respond, and the spinning will remain stable up to a certain well-defined speed. At this critical velocity, designated here $V_{1,m}$, the filaments begin to break in the bath near the face of the spinnerette. Spinning above this velocity is impossible, since none of the filaments can be removed from the bath continuously. This *maximum* first godet speed is very reproducible and depends on essentially every variable: e.g., polymer properties, spinning solution composition, bath composition, temperature, spinnerette, and Q.

As the first godet speed was increased in the experiment, the denier per filament of the final product, dpf, was decreased correspondingly, as seen by the material balance

$$\text{dpf} = 2.95 \times 10^4 \, (\rho w_2 Q / S V_1) \tag{1}$$

where S is the orientation stretch ratio, which is assumed constant here. Because there is a maximum possible first godet speed, then there is a minimum possible denier per filament for a given set of conditions.

The actual mechanism of this breakage, or instability, is undoubtedly quite complex. A rigorous analysis of the mechanics of wet-spinning would certainly be useful but very complex. Ziabicki in a series of papers has considered such an analysis for melt-spinning. The basic ideas can be applied to wet-spinning,[5] but very little useful information results, mainly because of the lack of rigor in considering all of the processes involved and their complexities. Ziabicki has also considered instabilities that can result.[6,7] Basically two types occur: breakup of the stream due to surface tension and a type of cohesive failure resulting from storage of elastic energy beyond a critical level during the attenuation of the unsolidified polymer solution or melt. The first type is usually not important in most fiber formation processes and certainly plays no significant role

here. The latter type, or cohesive failure, may be in part the operative mechanism of the instability observed here; however, there seems to be no way to demonstrate this. Ziabicki has worked out the conditions for cohesive failure for some very simple models, but the present system does not even approximate the conditions of his model, so these results will not be useful in analyzing the present data. We shall be content to investigate how various spinning variables affect $V_{1,m}$ and to attempt to relate these responses as fundamentally as possible to the basic phenomena that are known to be occurring. The rheological properties of the spinning solutions will be examined, since they contribute importantly to spinning behavior.

EXPERIMENTAL TECHNIQUES AND MEASUREMENTS

A single acrylonitrile–vinyl acetate copolymer was used throughout this work. It contained about 7.7% vinyl acetate by weight and had a $\bar{M}_w$ of 115,000, according to light scattering. This polymer was dissolved in dimethylacetamide (DMAc) to make spinning solutions of various solids levels, w_2. These solutions were pumped to the spinnerette from a storage tank by a Zenith pump. The spinnerette was fully immersed in the coagulation bath. The temperature and composition of this bath were controlled very closely to the desired level. A heat exchanger placed between the Zenith pump and the spinnerette was used to ensure that the spinning solution entering the spinnerette was at the bath temperature. Appropriate filters were also placed in this line. Except where noted, the spin bath had a composition of 55% DMAc in water by weight.

As indicated above, there are limitations imposed on the attenuation of filaments after they emerge from the spinnerette hole. As the filaments are taken away faster and faster, a point is reached where they break. Measurement of this maximum first godet speed is simple, but some care is required. The procedure begins by setting all conditions at a specified level and allowing the system to come to steady state. During this time the filaments are removed from the bath by the godet's running at a low speed. The speed is increased slowly until filaments begin to break. At this point the speed is lowered, and the loose filaments are rewrapped on the godet. A little time is allowed to determine whether spinning is stable at this speed. If it is not, the speed is reduced to a level where it is. If spinning is stable, the speed is increased until it is not. By slowly homing in it is possible to define accurately the transition speed from stable to unstable spinning within about 1 ft/min.

The average velocity of the spinning solution in the spinnerette hole, $\langle V \rangle$, is easily calculated from

$$\langle V \rangle = Q/(\pi/4)D^2 \tag{2}$$

where Q is the flow rate per hole and D is the hole diameter. If one observes the velocity at which the filament emerges from the hole under conditions of free extrusion (i.e., no godet takeup), it will be seen that this

velocity, V_f, is much smaller than $\langle V \rangle$. This is because the elasticity of the spinning solution permits it to store energy arising from the shearing in the capillary and the deformation on entering the capillary, which is released on emerging from the hole. The free velocity V_f plays a fundamental role in the problem of spinnability, so it has been measured extensively here. This was done by extruding filaments for a known period of time and measuring the length of the filaments produced.

An earlier publication[1] showed by model experiments that a very definite boundary exists between essentially coagulated and uncoagulated spinning solution as coagulation of the filament proceeds. The depth of penetration of this boundary, ξ, has been found to be proportional to the square root of the diffusion time during the initial stages of coagulation for cylindrical samples. For a given set of conditions the term $\xi/2t^{1/2}$ can be used to characterize the coagulation rate. This has proved to be a key fundamental variable in determining spinnability. It has been measured here for a few different coagulants. A more complete study of this factor for the DMAc–water system has been published.[1]

All of the spinnerettes used in this study were of a similar design, except in one group with unusually large capillary length-to-diameter (L/D) ratios. The usual spinnerette contained from 50 to 200 holes. Each hole had a conical counterbone with an included angle of about 45°. The capillary diameter was very uniform from hole to hole and was known very accurately. In the usual design the length of the capillary was just equal to its diameter: $L/D = 1$. The hole, or capillary, diameter D was consequently the only significant variable.

Spinnability as used here is influenced very much by the rheological properties of the spinning solution. The non-Newtonian viscosity of these solutions has been measured as a function of shear rate by well-known capillary viscometry techniques. An indication of solution elasticity can be determined from the size of the inlet corrections observed with the capillaries. The rheological data were obtained using capillaries that ranged in diameter from 12 to 125 mils.

RESULTS

Spinnerette Hole Diameter and Flow Rate

Figures 1 and 2 show the influences of both spinnerette hole diameter and the spinning solution flow rate per hole on the maximum first godet speed $V_{1,m}$ and the free velocity V_f, respectively, at 55°C for a 25% solution. Within certain limits other conditions give similar curves that are just numerically different. From these curves it is apparent that $V_{1,m}$ and V_f respond similarly to Q and D. Both the increase with Q and the decrease with D for each velocity can be rationalized, as will become apparent. The regularity of the responses shown in the first two figures is very appealing but does not represent the whole situation, for with smaller hole diameters a much more peculiar behavior is observed. For example,

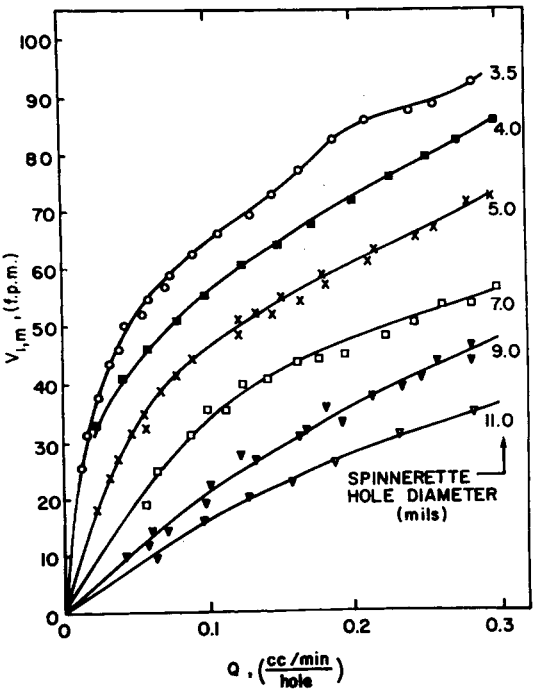

Fig. 1. Maximum first godet speed. Bath, 55% DMAc at 55°C. Spinning solution, 25% polymer.

Figure 3 shows both $V_{1,m}$ and V_f for a 3.0-mil diameter spinnerette for the conditions used in Figures 1 and 2. Initially both velocities increase with Q, but then a maximum appears in each curve, followed next by a minimum. It is significant that both $V_{1,m}$ and V_f show extreme values at the same Q. Smaller hole sizes at these conditions show a similar behavior. At other conditions, especially low temperatures, this complex maximum–minimum behavior is shown for hole diameters even larger than 3.0 mils. The influence of temperature and solids level on this peculiarity will be explored as well as the possible origin of this novel effect.

The similarity of $V_{1,m}$ and V_f in response to Q and D deserves a closer look. The shape of the curves in Figures 1 and 2 look almost the same. An even more striking similarity is seen in Figure 3. This figure also shows tension data[8] that are similar in behavior; this will be discussed later. This similarity in response suggests a plot of $V_{1,m}$ versus V_f, where each point represents the same Q and D. Such a plot is shown in Figure 4 for the data already discussed. There is a certain amount of scatter, but for the most part $V_{1,m}$ correlates with a V_f value regardless of the magnitude of D or Q; that is $V_{1,m} = f(V_f)$ even for the data in Figure 3. The free velocity is determined by both Q and D, but to a first approximation $V_{1,m}$ depends only on V_f. Similar reductions were found for other conditions with, of course, a different curve resulting for each set of conditions. This suggests that

we now have a means of separating spinnability into two parts: first, those things which affect V_f and, second, those things which affect the relationship between $V_{1,m}$ and V_f. It is tempting to say the V_f is influenced by events *inside* the spinnerette hole and that the relationship of $V_{1,m}$ to V_f is controlled by things happening in the spin bath. Later it will be seen that this is roughly but not strictly true.

The relationship between $V_{1,m}$ and V_f indicates how fast the filaments can be removed once V_f is established. We might think of $V_{1,m}/V_f$ as a maximum attenuation ratio. The results would be simpler if this ratio

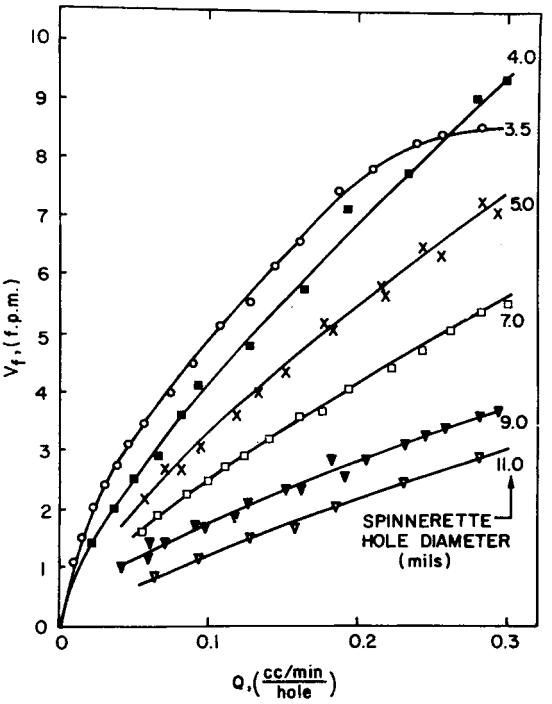

Fig. 2. Free velocity. Bath, 55% DMAc at 55°C. Spinning solution 25% polymer.

were a constant, but it is not. This ratio should have more fundamental significance than the normally used maximum jet stretch ratio, which is defined as $V_{1,m}/\langle V \rangle$. The breaking mechanism must be reflected in this relationship. We should expect this relationship to depend on the bath temperature, coagulation rate, spinning solution viscosity, and composition. These influences are primarily operative in the spin bath and not in the spinnerette hole.

It was suggested that V_f might be primarily determined by events occurring inside the spinnerette capillary. Consider a fluid to be forced through a hole of diameter D at a flow rate Q. For nonelastic Newtonian fluids, such as water, the smaller D is, the more momentum the fluid is

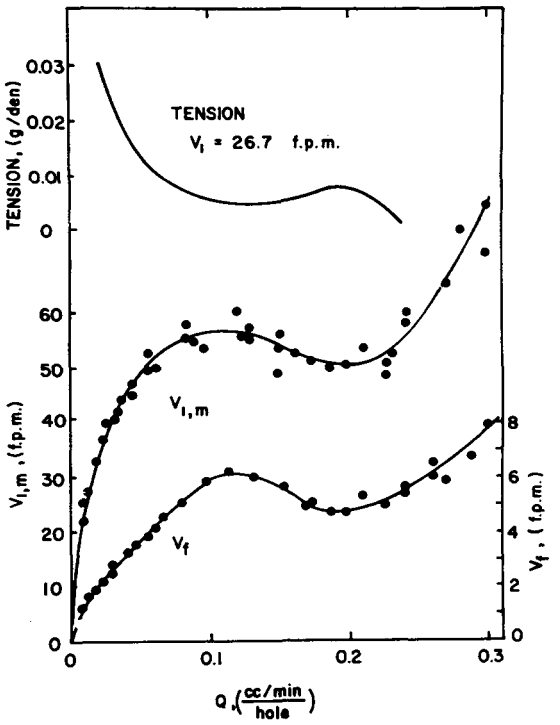

Fig. 3. Performance of a 3.0-mil spinnerette. Bath, 55% DMAc at 55°C. Spinning solution, 25% polymer.

given, so the faster it emerges from the hole. In this simple case it is easy to show that V_f would be

$$V_f = A\langle V \rangle \tag{3}$$

where A is 4/3 for long capillaries above very low Reynolds numbers[9] and $(\pi + 2)/\pi$ for a sharp-edged orifice.[10] Thus V_f can be increased by simply decreasing D for these fluids. However, for elastic fluids the situation is more complex because of the release of stored elastic energy as the fluid emerges from the capillary. This causes the stream of fluid to broaden or swell to a diameter D_f, which is larger than the capillary diameter D, that is, the well-known Barus effect. This swelling causes the fluid jet or filament to slow down. The diameters and velocities are related by

$$D_f/D = (\langle V \rangle / V_f)^{1/2} \tag{4}$$

if we consider D_f to be the diameter the filament would have if diffusional exchange with the bath did not alter the solids level or density of the filament. It should be pointed out that the swelling discussed here does not mean a composition change.

This elastic energy results from the deformation processes involved in entering the capillary plus those generated by the shear within the capil-

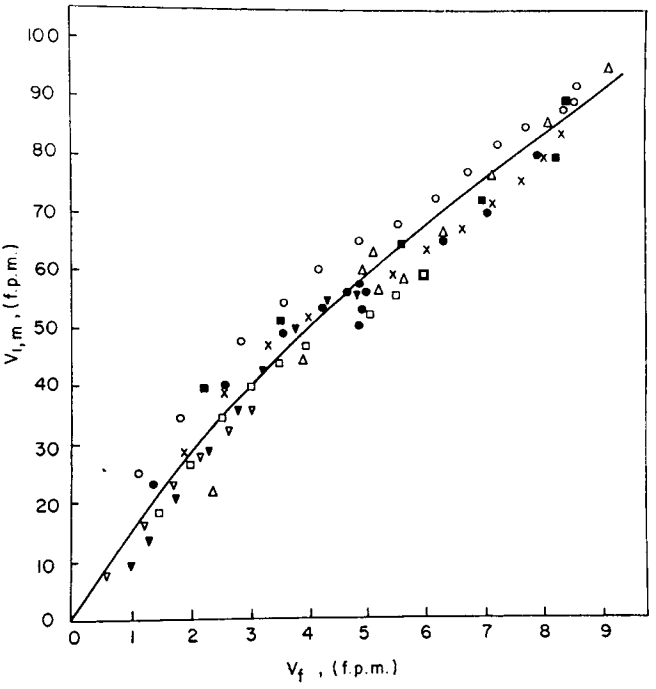

Fig. 4. Correlation of $V_{l,m}$ and V_f. Bath, 55% DMAc at 55°C. Spinning solution, 25% polymer. Symbols indicate spinnerette size; see Figures 1, 2, and 3 for code.

lary. Thus D_f/D should depend on the spinnerette hole design, the shear rates involved, the rheological properties of the spinning solution, temperature, etc. The amount of swelling observed in any given situation will depend on all of these factors plus the environment into which the filaments are extruded, depending on what restraints the environment can have on the swelling process. For now we can consider that there is a maximum or equilibrium value of D_f/D, but this amount of swelling may not be realized, because of these restraints. This question will be explored more fully.

The free-velocity data in Figures 2 and 3 were converted into a jet swell ratio D_f/D via eq. (4). For each temperature, spinning solution, and bath this ratio should be a function of the shear conditions inside the hole. A simple method of expressing these conditions is to use the apparent shear rate at the capillary wall; that is:

$$\dot{\gamma}_{wa} = 4Q/\pi R^3 \tag{5}$$

where R is the capillary radius, or $^1/_2D$. Figure 5 shows that $\dot{\gamma}_{wa}$ adequately reduces the V_f, Q, and D data into a single curve for this case. In these experiments two important variables have not been changed: namely, hole design and coagulation rate.

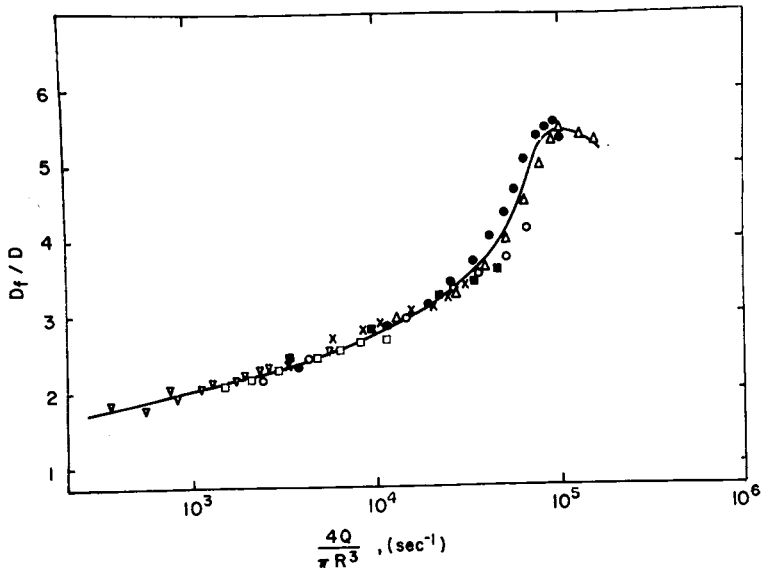

Fig. 5. Shear rate dependence of jet swell. Bath, 55% DMAc at 55°C. Spinning solution, 25% polymer. Symbols indicate spinnerette size; see Figures 1, 2, and 3 for code.

The very steep rise in D_f/D just above 10^4 sec^{-1} is an interesting feature that can be used to rationalize the maximum–minimum behavior observed in V_f versus Q and, hence, $V_{1,m}$ versus Q. First it is necessary to think of the relation D_f/D versus $\dot{\gamma}_{wa}$ as a fundamental property of the spinning solution just as, for example, its viscosity is. It is quite easy to show from eq. (4) that

$$[d \ln (D_f/D)]/[d \ln \dot{\gamma}_{wa}] = {}^1/_2[1 - (d \ln V_f)/(d \ln Q)] \qquad (6)$$

for a given hole size. This equation predicts that a maximum will occur in V_f versus Q if the slope of a plot of ln (D_f/D) versus ln $\dot{\gamma}_{wa}$ exceeds $^1/_2$ in this range of shear rates. Likewise, a minimum will occur if the slope drops below $^1/_2$, again as the shear rate increases. This allows an after-the-fact explanation to be advanced for the peculiar behavior noted earlier. In Figures 2 and 3 the flow rate range is the same for all hole sizes, but the shear rate ranges are quite different. To exemplify this point, recall that at 55°C, for instance, a 3.0-mil spinnerette shows the maximum–minimum behavior, but a 5.0-mil jet does not. A glance at Figure 5 shows that for the Q range used the 3.0-mil spinnerette extends into this steep region, whereas the 5.0-mil does not. At 30°C this behavior was found in larger hole sizes than at 55°C. A plot similar to Figure 5 for 30°C shows that the steep rise occurs at lower shear rates at this lower temperature. However, the relation at 30°C is numerically identical with that at 55°C up to about 10^4 sec^{-1}. This suggests that a maximum and a minimum would be observed at 55°C for a 5.0-mil spinnerette if the flow rate were high

enough. In summary it is clear that the free-velocity anomaly can be rationalized in terms of shear rate considerations.

Fitzgerald and Craig[2] tentatively suggested a correlation between $V_{1,m}$ and Q/D^2. The latter term is proportional to $\langle V \rangle$. The data given here show that this correlation is valid in some regions but breaks down in others. For example, most of the data in Figure 1 form a single curve when $V_{1,m}$ is plotted against $\langle V \rangle$; however, this is not true of the data in Figure 3 or of any of the data at 30°C. It is believed that the V_f correlation is more general and more significant fundamentally. Actually, $V_{1,m}$ correlates with $\langle V \rangle$ only when D_f/D is essentially constant, in which case $\langle V \rangle$ is proportional to V_f, making an apparent relationship.

To sum up, the effect of spinnerette hole diameter on V_f and, thus, on $V_{1,m}$ represents a balance between momentum and shear rate or elastic energy considerations. At constant Q momentum increases as D decreases but so does the shear rate and, hence, the amount of jet swell. The net effect is an optimum hole size, where V_f and $V_{1,m}$ are maximum for a given Q. In most cases these maxima occur at roughly 3–4 mils.

Temperature

In part the effect of bath and spinning solution temperature has already been seen. However, it will be informative to take a closer look especially

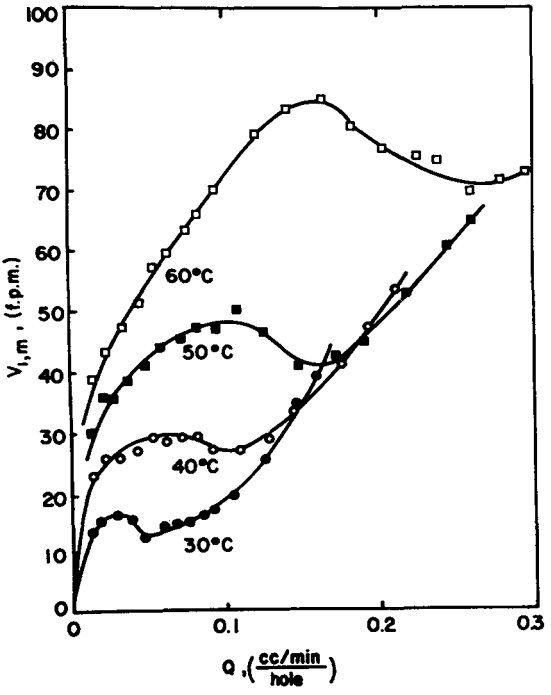

Fig. 6. Effect of temperature on maximum first godet speed for a 3.0-mil spinnerette. Bath, 55% DMAc at 55°C. Spinning solution, 25% polymer.

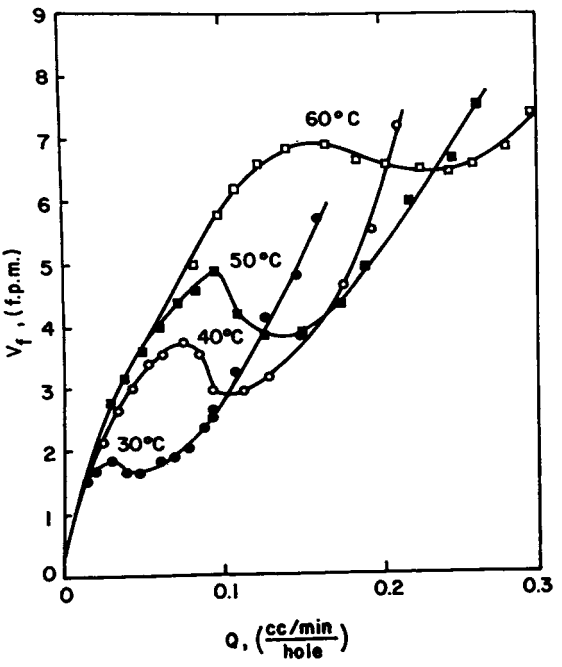

Fig. 7. Effect of temperature on free velocity for a 3.0-mil spinnerette. Bath, 55% DMAc at 55°C. Spinning solution, 25% polymer.

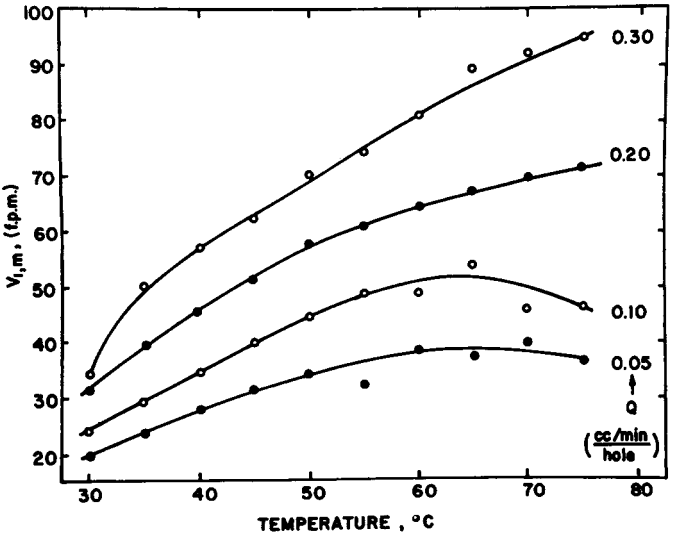

Fig. 8. Effect of temperature on maximum first godet speed for a 5.0-mil spinnerette. Bath, 55% DMAc at 55°C. Spinning solution, 25% polymer.

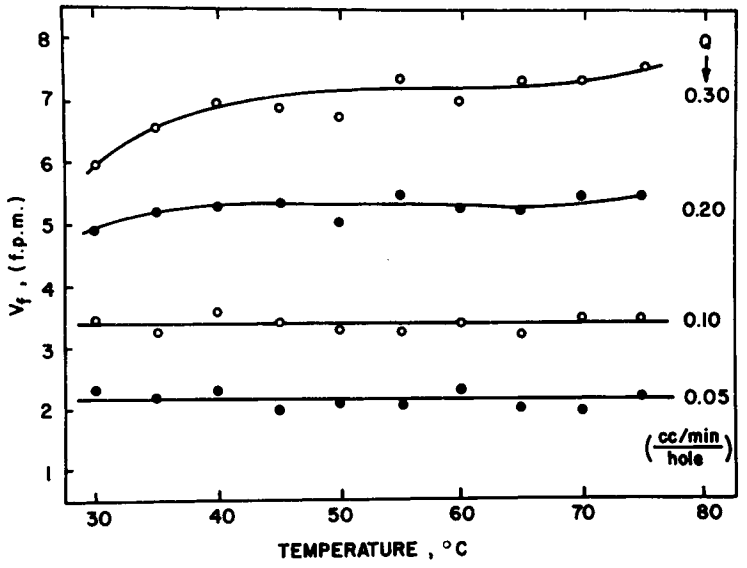

Fig. 9. Effect of temperature on free velocity for a 5.0-mil spinnerette. Bath, 55% DMAc at 55°C. Spinning solution, 25% polymer.

in the shear rate region where D_f/D is sensitive to temperature. This is illustrated nicely by studying 3.0-mil and 5.0-mil spinnerettes at the same flow rates.

Figures 6 and 7 show $V_{1,m}$ and V_f versus Q for a 3.0-mil spinnerette at various temperatures. A maximum and minimum appear in both $V_{1,m}$ and V_f at each temperature, the positions of these extreme values being highly temperature-sensitive. As before, both $V_{1,m}$ and V_f show their maxima and minima at approximately the same flow rates. The free-velocity data in Figure 7 can be reduced to a plot of D_f/D versus $4Q/\pi R^3$. A family of curves results, each isotherm being different at shear rates above about 10^4 sec^{-1}, but each merges into a common curve below this value.

The response to temperature of 5.0-mil spinnerettes is entirely different, since no maxima–minima behavior is observed in the range from 30 to 75°C. Figures 8 and 9 show the dependence of $V_{1,m}$ and V_f on temperature for four levels of Q. At high flow rates $V_{1,m}$ simply increases with temperature as one would expect; however, at low flow rates $V_{1,m}$ tends to show a maximum. For some reason the data are very difficult to reproduce in this particular region; hence, it is not possible to pin down the behavior exactly. The V_f data are very surprising, since there is very little effect of temperature. At low flow rates the points fall randomly about a line of constant V_f, whereas at higher flow rates a small but significant increase with temperature is discernible at low temperatures. This illustrates again the contrasting temperature dependence in different ranges of shear rate. As shown in Figures 8 and 9, the responses of $V_{1,m}$ and V_f to temperature are

quite different, but this does not invalidate the cause-and-effect relationship between them suggested earlier. It must be remembered that $V_{1,m}$ versus V_f is temperature-dependent; in fact, a plot such as Figure 4 exists for each temperature.

Coagulation Rate

In polymer melt extrusion it is generally known that the quenching conditions can influence the amount of jet swell, D_f/D. A similar effect might be anticipated for fiber extrusion into a bath where rapid mass transfer can take place, since mass transfer in solution systems plays a role equivalent to heat transfer in melt systems. To illustrate this effect, the coagulation rate $\xi/2t^{1/2}$, was measured for seven different coagulants by the procedure referred to earlier.[1] The initial linearity of the boundary penetration ξ in the square root of the diffusion time for cylindrical specimens is illustrated in Figure 10. The coagulation rates are tabulated in Table I.

TABLE I
Coagulation Rates at 40°C for Various Coagulants

Coagulant	$\xi/2t^{1/2}$ ($\times 10^3$), cm/sec$^{1/2}$
Chloroform	2.91
Carbon tetrachloride	1.06
t-Butyl alcohol	1.59
Methanol	2.95
Benzene	1.24
Water	3.22
Ethylene glycol	1.23

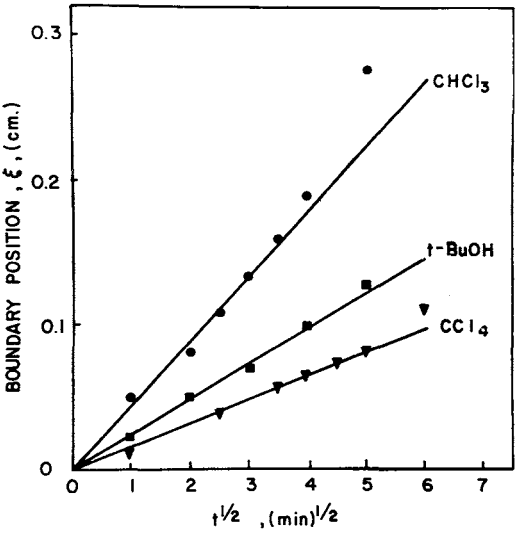

Fig. 10. Coagulation rates at 40°C. Spinning solution, 25% polymer. Samples were rods with a radius of 0.467 cm.

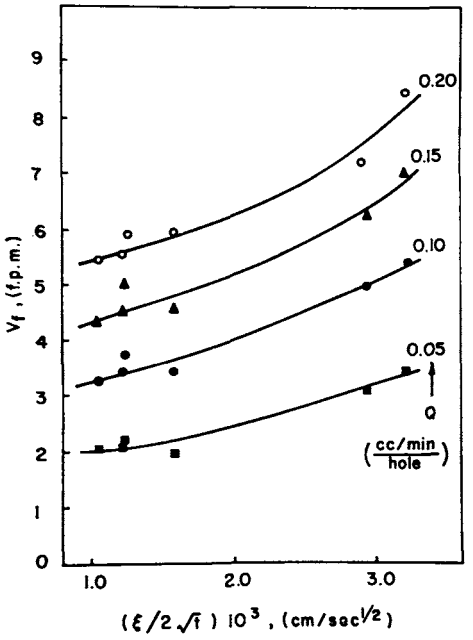

Fig. 11. Effect of coagulation rate on free velocity at 40°C for a 5.0-mil spinnerette. Spinning solution, 25% polymer.

These measurements were made at 40°C with 25% spinning solutions. Spinnability data were obtained in each coagulant at 40°C for comparison with these results.

Figure 11 shows clearly that V_f (at constant Q) does increase as the coagulation rate is increased. The reason for this is easily outlined. After the spinning solution is extruded, it would enlarge to an equilibrium D_f/D value, except that, because of the coagulation, a skin begins to grow, which acts as a restraint to the swelling. Since the filament cannot swell as much as it would like to, it issues with a faster velocity. It seems only reasonable that, the faster the skin is formed, the larger will be the quenching effect and so the larger the V_f.

The relation between V_f and coagulation rate was as expected. However, we are faced with a more complex behavior when $V_{1,m}$ is compared with coagulation rate data. First, it is known that if all else is the same, an increase in V_f leads to an increase in $V_{1,m}$; however, when the coagulation rate is changed, it should be expected that the relation between $V_{1,m}$ and V_f will be altered. General considerations would lead one to think that for a given V_f the $V_{1,m}$ would decrease as the coagulation rate increases and, in fact, the data show this when compared in this way. So it appears that there will be two competing processes as $\xi/2t^{1/2}$ increases. The data in Figure 12 confirm this reasoning; for, although the data are somewhat scattered, it is relatively safe to conclude that $V_{1,m}$ goes through a minimum when compared at constant Q. The minimum is caused by the competi-

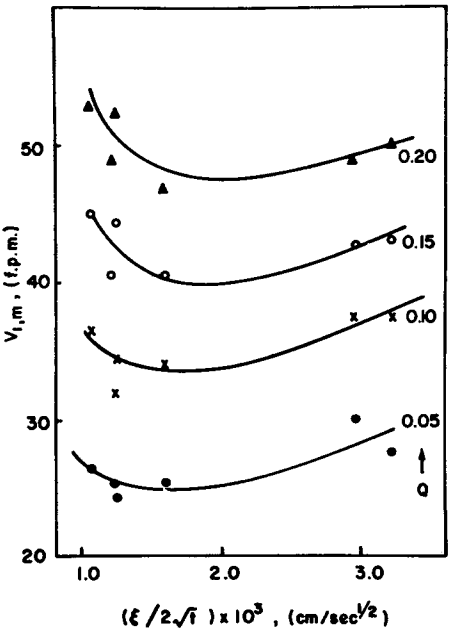

Fig. 12. Effect of coagulation rate on maximum first godet speed at 40°C for a 5.0-mil spinnerette. Spinning solution 25% polymer.

tion of the two opposing factors mentioned above. At high coagulation rates the effect on V_f is dominant, while at low coagulation rates the effect on the ratio of $V_{1,m}$ to V_f is dominant. The results in Figure 12 would, admittedly, be more convincing if there were a larger number of points more equally distributed on the abscissa; however, this would have been very difficult to achieve.

The author does not believe that the scatter in Figure 12, for example, represents actual errors necessarily; instead, it may indicate that all of the behavior cannot be characterized by a single parameter such as $\xi/2t^{1/2}$. For a complete description it would be necessary to consider, for example, the strength or modulus of the skin formed and so forth. The use of $\xi/2t^{1/2}$ does, however, illustrate the point to be made, namely, that both the rheological and diffusional phenomena must be considered.

Spinning Solution Composition

Thus far all of the results reported have been for spinning solutions containing 25% polymer. In this section the solids level will be varied from 20 to 28%. We can expect to see the free velocity and the relationship between V_f and $V_{1,m}$ altered.

Figure 13 shows the effect of solids level on $V_{1,m}$ versus Q at 55°C for a 3.0-mil spinnerette. Under these conditions no maxima are observed at 20 and 23% for the flow rates considered, but very definite maximum

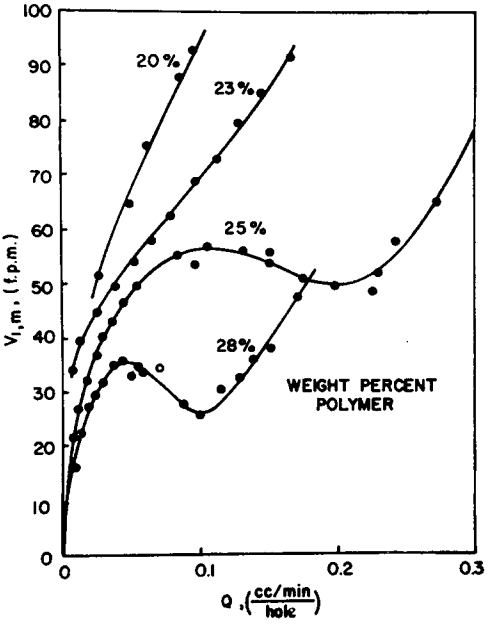

Fig. 13. Influence of spinning solution composition on maximum first godet speed for a 3.0-mil spinnerette. Bath, 55% DMAc at 55°C.

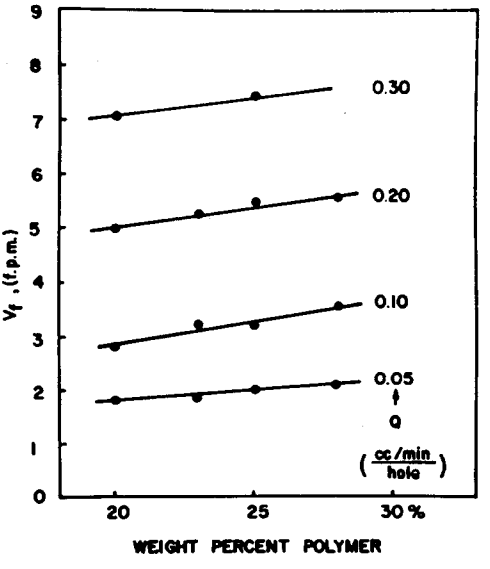

Fig. 14. Influence of spinning solution composition on free velocity for a 5.0-mil spinnerette. Bath, 55% DMAc at 55°C.

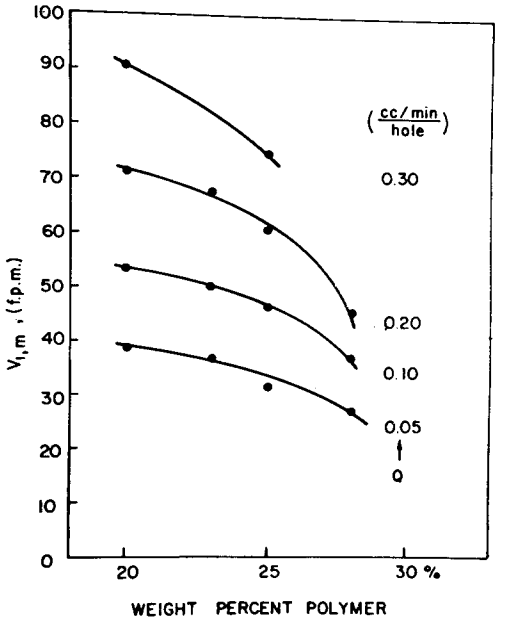

Fig. 15. Influence of spinning solution composition on maximum first godet speed for a 5.0-mil spinnerette. Bath, 55% DMAc at 55°C.

and minimum is seen for both 25 and 28%. The transition lies somewhere between 23 and 25%. Free-velocity plots are quite like those shown in Figure 13. Similar data at 30°C indicate a maximum and minimum for each solids level, including 20% for the 3.0-mil spinnerette.

The trends in V_f and $V_{1,m}$ caused by solids level for a 5.0-mil spinnerette are shown in Figures 14 and 15, where both are plotted against the solids level at constant values of Q. It is quite surprising at first to see that V_f increases as the polymer content increases. Since the viscosity increases markedly with increases in polymer concentration, one first expects large increases in the elastic contribution. However, the data do not seem to show this expectation. Of course, it must be remembered that the coagulation rate has a very strong influence on D_f/D, and it may be changing with solids enough to reverse the expected trend. To see whether this strange situation could be resolved in this way, the jet swell was measured visually in air for 20 and 25% solutions. These observations showed that indeed the swelling is larger for the 25% solution, as one would intuitively expect. Thus the trend in Figure 14 must be due to the coagulation rate. This would indicate an increase in coagulation rate as the solids level increases.

Capillary Length

Up to this point the only independent spinnerette variable has been the hole diameter, since the capillary L/D was set at approximately 1. The

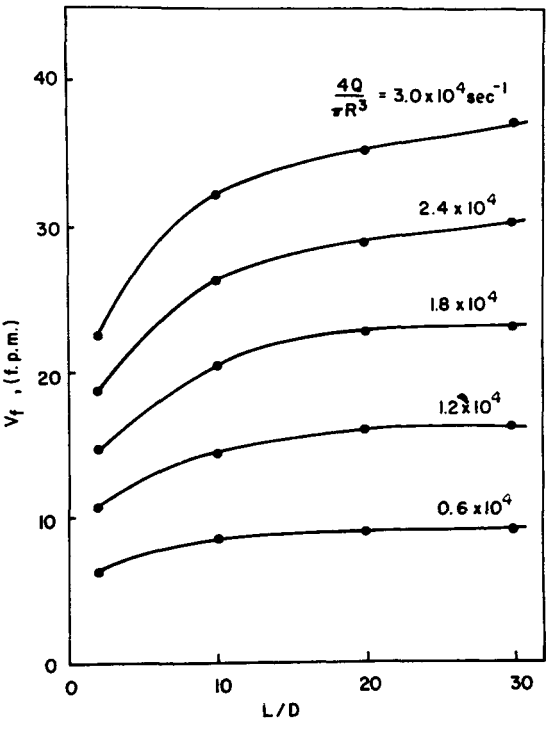

Fig. 16. Effect of capillary L/D on free velocity. Capillary diameter, 12 mils. Bath, 55% DMAc at 55°C. Spinning solution, 25% polymer.

L/D ratio is widely recognized as an important die design variable for plastics extrusion. Repeatedly the amount of jet swell, D_f/D, has been shown to decrease as the capillary is made longer.[11] This effect was explored here by use of a series of single-hole 12-mil-diameter capillaries that had L/D's of 2, 10, 20, and 30. This reduction in the jet swell, or Barus effect, is illustrated in Figure 16 for the system studied here. The data are presented in terms of free velocity rather than D_f/D but, of course, the two are related by eq. (4). The reduced swelling at longer capillary lengths results in an increased free velocity. A certain swelling ratio can be expected for a given set of conditions and L/D, owing to the elastic deformation processes occurring upon entering the capillary plus a contribution from the normal stresses that would exist under equilibrium flow at the same shear rate. For a sharp-edged orifice, i.e. $L = 0$, each of these would make a maximum contribution and, thus, a high D_f/D and a low V_f. As the capillary gets longer, time is allowed for relaxation of the stresses generated by the entrance deformation and, presumably, with a long enough tube this entrance effect would be completely forgotten. The curves at low shear rates in Figure 16 are almost flat at an L/D of 30. The flow rates have been adjusted to high levels, so that the shear rates would be almost comparable to those found in the 3.0-mil and 5.0-mil spinnerettes.

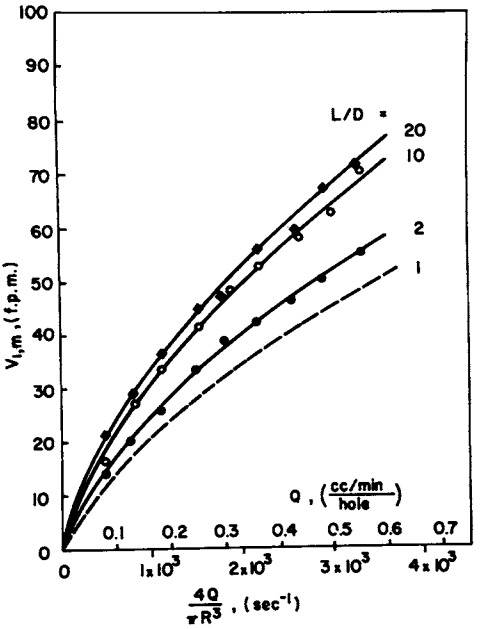

Fig. 17. Effect of capillary L/D on maximum first godet speed. Capillary diameter 12 mils. Bath, 55% DMAc at 55°C. Spinning solution, 25% polymer.

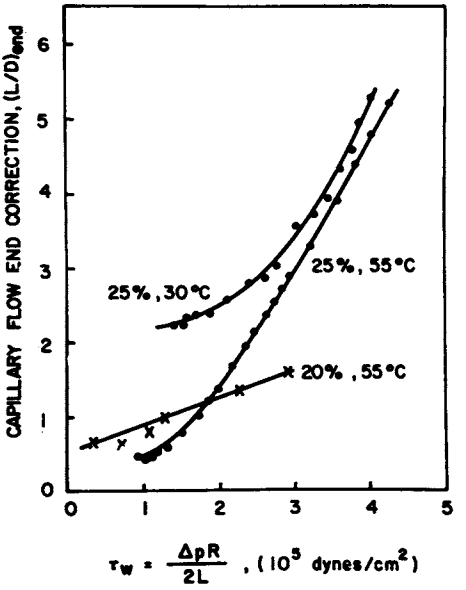

Fig. 18. End corrections for pressure drop in capillary flow for spinning solutions. Compositions and temperatures as indicated.

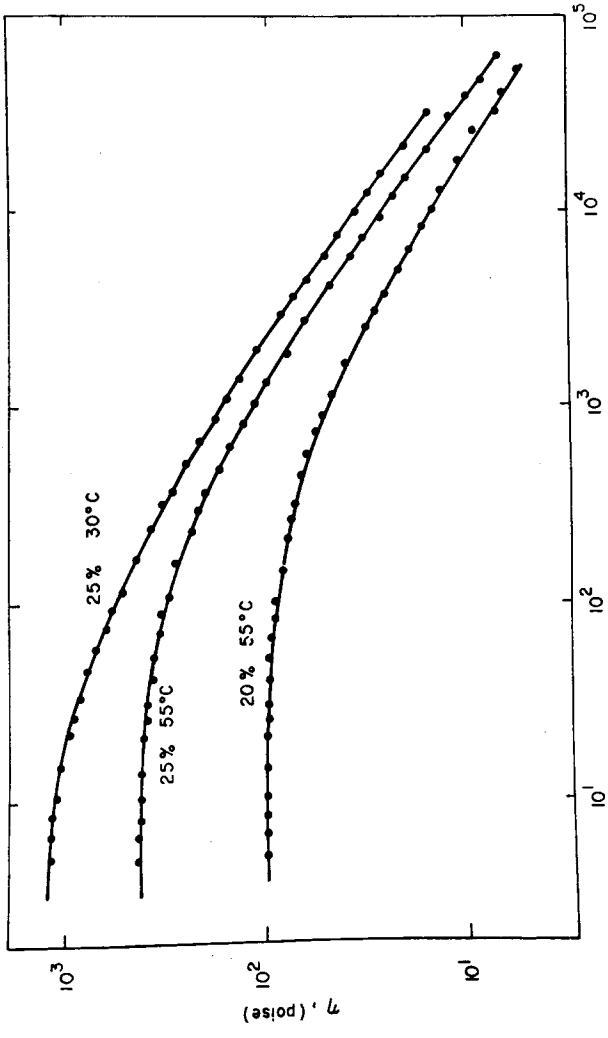

Fig. 19. Non-Newtonian viscosity of spinning solutions. Compositions and temperatures as indicated.

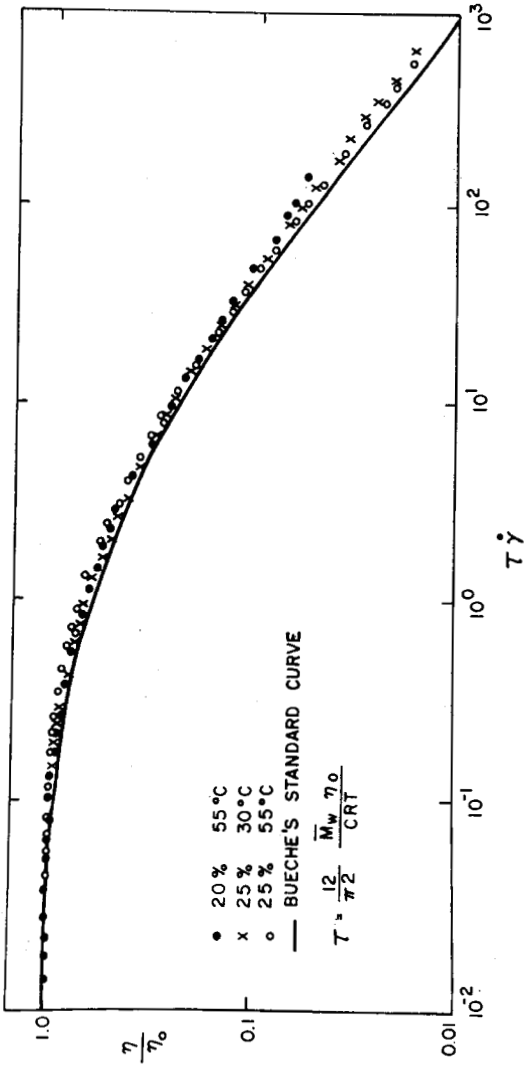

Fig. 20. Reduced non-Newtonian viscosity plot.

Earlier it was shown that if V_f is increased in some way, then a corresponding increase in $V_{1,m}$ can usually be expected. Maximum first godet speed data using the same series of 12-mil capillaries confirm this, as shown in Figure 17. Here $V_{1,m}$ is plotted against Q and, hence, $\dot{\gamma}_{wa}$ for three of these capillaries. Owing to limitations in godet speeds, the flow rates and, hence, shear rates in Figure 17 are lower than those in Figure 16 by a factor of about 10. Despite this, similar trends may be expected. The characteristic curve for an L/D of 1 has been estimated from data in Figure 1 by using the relation between $V_{1,m}$ and $\langle V \rangle$, which is valid at low shear rates at 55°C.

Rheological Properties of Spinning Solutions

Fitzgerald and Craig[2] measured the non-Newtonian viscosity over a limited range of shear rates for spinning solutions similar to those used here. Their results do not extend to low enough shear rates to give the constant viscosity that prevails in the very low shear rate region, where a Newtonian flow regime exists. This lower limiting viscosity η_0 is a most important rheological parameter, which would be helpful for interpreting spinnability results. Capillary tubes of various dimensions offer a relatively easy way of measuring the viscosity over several decades of shear rates, so this approach was used to get the desired information. Pressure drop Δp versus flow rate Q for these tubes was obtained. To reduce this to fundamental information about the non-Newtonian viscosity η, two types of correction were made.

The first was an end correction which arises from both viscous and elastic contributions from the velocity profile rearrangement that the solution experiences upon entering the capillary. This term can be expressed as an equivalent length $(L/D)_{\text{end}}$. It was determined by procedures originally outlined by Bagley.[12] The corrections evaluated for some of the solutions employed here are shown in Figure 18, plotted against the shear stress at the tube wall, τ_w:

$$\tau_w = \Delta pR/2L \tag{7}$$

It is interesting to see the effect of temperature and composition on these values. The second was the Rabinowitsch correction,[9] which accounts for the fact that the shear rate at the tube wall, $\dot{\gamma}_w$, is not $4Q/\pi R^3$ for non-Newtonian fluids but is related by

$$\dot{\gamma}_w = \dot{\gamma}_{wa}[{}^3/_4 + {}^1/_4(d \log \dot{\gamma}_{wa})/(d \log \tau_w)] \tag{8}$$

After these corrections were made, the viscosity η was calculated from the ratio $\tau_w/\dot{\gamma}_w$. The complete results for three sets of measurements are shown in Figure 19. The region where η is constant, i.e. η_0, is apparent.

Bueche[13] has suggested that a single master curve should result if η/η_0 is plotted against $\tau\dot{\gamma}$, where

$$\tau = (12/\pi^2)(\bar{M}_w\eta_0/CRT) \tag{9}$$

and C is the concentration of polymer in grams per cubic centimeter. Such a plot was made from the data in Figure 19; the final result is shown in Figure 20. The points are the experimental data, which form a single curve very nicely. Note that in the calculations the weight-average molecular weight is used, and light-scattering results indicate it is 115,000 for this polymer. The solid line is a curve Bueche found by studying a large number of systems. This curve agrees remarkably well with the experimental data given here. Almost perfect agreement would exist if a $\bar{M}_w$ of about 100,000 were used in calculating τ.

Since the entire shear rate dependence of the viscosity can be predicted in this way, there is no reason to measure anything but the lower limiting value η_0. This was done over a range of concentrations and temperatures, with the results given in Table II. Calculated values of τ are also given

TABLE II
Summary of Rheological Data

Polymer, wt-%	Temp., °C	η_0, P	τ, msec
20	30	314	8.95
20	55	100	2.64
23	30	700	17.4
23	55	233	5.34
25	30	1250	28.4
25	55	421	8.86
28	30	2650	53.9
28	55	1190	22.4

for each condition. Theoretically, τ is the longest relaxation time in a spectrum of relaxation times for the viscoelastic solution. Other theories[14] predict a similar group of terms for the terminal relaxation time, but with a numerical factor of $6/\pi^2$ instead of $12/\pi^2$. There seems to be no way to decide which numerical factor should be used to best predict relaxation times; however, for the purposes used in Figure 20 it is arbitrary which is used, so long as the use is consistent.

DISCUSSION

The obvious questions now are how and why the filaments break catastrophically at the critical speed $V_{1,m}$. A large collection of information has been given here, but it does not give the fundamental mechanism directly. However, a general mechanism will be postulated now, one that seems to agree with the facts. Tension in the filaments near the spinnerette face is the reason for the failure. The existence of this tension is well known, but its causes are not, so we should first explore the origin of the tension. Even in the absence of surface tension a certain tension would be required to attenuate a liquid filament into a filament of smaller diameter, because of the viscosity of the fluid. This is the Trouton experi-

ment. Now if this liquid were viscoelastic instead of just viscous, additional tension would be required to balance the elastic forces. A similar attenuation occurs during spinning. A filament of polymer solution is extruded from a hole, and then the filament is pulled on to make its diameter smaller. Of course, during spinning coagulation occurs. As indicated earlier, coagulation proceeds by a moving boundary that starts at the surface and advances inward, leaving a solid structure behind. Thus coagulation in effect imposes a boundary condition on the filament, since it determines the length and shape of the fluid region. Assuming that most of the attenuation occurs in the fluid region, less tension will be required, the longer the fluid region (or the slower the coagulation), because the effective extension or acceleration rate is less. Another source of filament tension is hydrodynamic drag. Its contribution to the tension is very small near the spinnerette but increases along the filament to a maximum at the exit of the bath. Observations show the filaments break very near the spinnerette face, where the hydrodynamic drag forces are minimal, so it appears that this source can be ignored.

Spinning solution elasticity makes an additional contribution to the tension through the Barus effect. If the solution issued from the hole at a speed close to $\langle V \rangle$, then very little filament attenuation would be necessary, since frequently V_1 is not much different and is even less in some cases. But because of the Barus effect the solution comes out with a velocity V_f, much less than $\langle V \rangle$, if no tension is applied; hence, a larger acceleration is required to get the filament speed up to V_1. The influence of V_f on tension is shown very dramatically in Figure 3. The upper curve is the tension[8] in grams per denier, where the denier is that on the first godet. These data include the hydrodynamic contribution. In this case V_1 was held constant at 26.7 ft/min, while Q was varied; thus, V_f changed according to the lower curve. The tension goes through extreme values at the same Q as V_f does. When V_f is high, the tension is low and vice versa, just as one might expect on the basis of the changes in extension rates.

Now that the origin of the tension is established, where and how does this lead to filament breakage? Every indication points to the partially coagulated region. A filament cross section would show an uncoagulated, fluid core surrounded by a coagulated, solid sheath, or skin, the core diameter decreasing as the plane of cross section gets further away from the spinnerette. The filament tension is transmitted to this region, and there seem to be two likely ways of breaking the filament continuity when the tension becomes too great. There is undoubtedly some shearing motion within the fluid core, caused by transmission of a shear stress across the solid–liquid boundary. One mechanism of failure would be separation of this solid–liquid boundary through a telescopic type of motion. A second possibility would be the rupture of the skin because of an excessive tensile stress there. Once this occurred, the filament would break, since the fluid core could not support all of the tension. For this mode it is easy to see how the structure of the coagulated filament (controlled by coagulation

conditions) could be important in determining $V_{1,m}$. There are certainly other mechanisms that one could postulate, but the point of view given above seems adequate for the present time. This model helps us to see the interacting role of spinning solution viscosity, elasticity, and coagulation factors and how they determine spinnability. It would be interesting to isolate experimentally each of these phenomena and their effect on spinnability, but this does not seem possible, as one can see by the following. As the composition of the spinning solution and the extrusion temperature are changed, the viscosity changes. The tension in the filaments therefore changes also. If the viscosity were the only factor to consider, then the maximum first godet speed (for a given spinnerette, pump rate, and bath) would be a single function of the viscosity. If such an attempt is made to correlate $V_{1,m}$ with the η_0 data in Table II, it is readily seen that this is not true. The data approach a single curve in some regions but diverge greatly in others. Obviously, elasticity and coagulation variables must also be considered, since they have not remained constant.

The rheological data combined with Bueche's theory permit the estimation of the longest relaxation time in the relaxation time spectrum for the viscoelastic spinning solutions. These calculated times are shown in Table II. It will be informative to compare them with the average residence time t of the spinning solution in the capillary. This residence time is given by

$$t = 8(L/D)/\dot{\gamma}_{wa} \tag{10}$$

Typical conditions that have been used here are $\dot{\gamma}_{wa} \approx 10^4$ sec^{-1} and $L/D = 1$, so $t \approx 1$ msec. In most cases the longest relaxation time is greater than the average residence time in the region of high shear. This helps to explain the large effects observed here.

The author expresses his appreciation to the Chemstrand Research Center for permission to publish this work and to Z. P. Whitfield, who helped obtain most of the experimental data.

References

1. D. R. Paul, *J. Appl. Polymer Sci.*, **12**, 383 (1968).
2. W. E. Fitzgerald and J. P. Craig, *Am. Chem. Soc. Polymer Preprints*, **7**(2), 742 (1966).
3. J. P. Knudsen, *Textile Res. J.*, **33**, 13 (1963).
4. J. P. Craig, J. P. Knudsen, and V. F. Holland, *Textile Res. J.*, **32**, 435 (1962).
5. W. C. Brinegar and M. E. Epstein, *Am. Chem. Soc. Polymer Preprints*, **7**(2), 805 (1966).
6. A. Ziabicki and R. Takserman-Krozer, *Kolloid-Z.*, **198**, 60 (1964).
7. A. Ziabicki and R. Takserman-Krozer, *Roczniki Chem.*, **38**, 653 (1964).
8. W. E. Fitzgerald, private communication.
9. J. M. McKelvey, *Polymer Processing*, Wiley, New York, 1962, Ch. 3.
10. H. Lamb, *Hydrodynamics*, Dover, First American Edition, New York, 1945, p. 99.

11. T. Arai and H. Aoyama, *Trans. Soc. Rheol.*, **7**, 333 (1963).
12. E. B. Bagley, *J. Appl. Phys.*, **28**, 624 (1957).
13. R. Bueche and S. W. Harding, *J. Polymer Sci.*, **32**, 177 (1958).
14. J. D. Ferry, *Viscoelastic Properties of Polymers*, Wiley, New York, 1961, Ch. 10.

Received March 18, 1968
Revised April 30, 1968